

Three Ways to Improve Semantic Segmentation with Self-Supervised Depth Estimation

Lukas Hoyer
ETH Zurich

lukas.hoyer@outlook.com

Dengxin Dai
ETH Zurich

dai@vision.ee.ethz.ch

Yuhua Chen
ETH Zurich

yuhua.chen@vision.ee.ethz.ch

Adrian Köring
University of Bonn

adrian.koering@uni-bonn.de

Suman Saha
ETH Zurich

suman.saha@vision.ee.ethz.ch

Luc Van Gool
ETH Zurich & KU Leuven

vangool@vision.ee.ethz.ch

Abstract

Training deep networks for semantic segmentation requires large amounts of labeled training data, which presents a major challenge in practice, as labeling segmentation masks is a highly labor-intensive process. To address this issue, we present a framework for semi-supervised semantic segmentation, which is enhanced by self-supervised monocular depth estimation from unlabeled images. In particular, we propose three key contributions: (1) We transfer knowledge from features learned during self-supervised depth estimation to semantic segmentation, (2) we implement a strong data augmentation by blending images and labels using the structure of the scene, and (3) we utilize the depth feature diversity as well as the level of difficulty of learning depth in a student-teacher framework to select the most useful samples to be annotated for semantic segmentation. We validate the proposed model on the Cityscapes dataset, where all three modules demonstrate significant performance gains, and we achieve state-of-the-art results for semi-supervised semantic segmentation. The implementation is available at https://github.com/lhoyer/improving_segmentation_with_selfsupervised_depth.

1. Introduction

Convolutional Neural Networks (CNNs) [35] have achieved state-of-the-art results for various computer vision tasks including semantic segmentation [40, 5]. However, training CNNs typically requires large-scale annotated datasets, due to millions of learnable parameters involved. Collecting such training data relies primarily on manual annotation. For semantic segmentation, the process can be extremely costly, due to the required dense annotations.

For example, annotating a single image in the Cityscapes dataset takes on average 1.5 hours [9].

Recently, self-supervised learning has shown to be a promising replacement for manually labeled data. It aims to learn representation from the structure of unlabeled data, instead of relying on a supervised loss, which involves manual labels. The principle has been successfully applied in depth estimation, for stereo pairs [16] or image sequences [74].

On the other hand, semantic segmentation is known to be tightly coupled with depth. Several previous works have reported that jointly learning semantic segmentation and *supervised* monocular depth estimation can benefit the performance of both tasks [62], which suggests that the correlation between these tasks can be a powerful source to learn better representations.

Motivated by these two observations, we investigate the question, *how can we leverage the self-supervised depth to improve semantic segmentation?*

In this work, we propose a threefold approach to utilize self-supervised monocular depth estimation (SDE) [16, 74, 17] to improve the performance of semantic segmentation and to reduce the amount of annotation needed. First, we learn SDE as auxiliary task for semantic segmentation and show that both transfer learning [49] and multi-task learning [72] noticeably improve the performance of semantic segmentation. Second, we propose a strong data augmentation strategy, *DepthMix*, which blends images as well as their labels according to the structure of the scenes obtained from SDE. In comparison to previous methods [70, 47], *DepthMix* explicitly respects the geometric structure of the scenes and generates fewer artifacts (see Fig. 1). And third, we propose an *Unsupervised Data Selection for Annotation*, which automatically selects the most useful samples to be annotated in order to maximize the gain. The selection is driven by two criteria: *diversity* and *uncertainty*. Both of them are conducted by a novel use of SDE in this context.

In contrast to regular active learning [54, 67], this approach does not require a human in the loop. Specifically, we do not use any semantic segmentation labels during the whole selection process. This greatly improves the flexibility and efficiency of the method.

The main advantage of our method is that we can learn from a large base of unlabeled image sequences and utilize the learned knowledge to improve semantic segmentation performance in various ways. In our experimental evaluation on Cityscapes [9], we demonstrate significant performance gains of all the three components and improve the previous state-of-the-art for semi-supervised segmentation by a considerable margin. Specifically, our methods achieves 93% of the full annotation baseline performance with only 1/30 available labels and even outperforms it with 1/8 labels. Our contributions summarize as follows:

- (1) To the best of our knowledge, we are the first to utilize SDE based on image reconstruction to exploit unlabeled image sequences and significantly improve semi-supervised semantic segmentation performance.
- (2) Furthermore, we propose *DepthMix*, a strong data augmentation strategy, which respects the geometry of the scene and achieves, in combination with (1), state-of-the-art results for semi-supervised semantic segmentation on Cityscapes.
- (3) Finally, we propose an *Unsupervised Data Selection for Annotation* based on SDE. In contrast to active learning, we do not require semantic segmentation annotations during the whole data selection process. To the best of our knowledge, we are the first studying unsupervised data selection for semantic segmentation.

2. Related Work

2.1. (Semi-Supervised) Semantic Segmentation

Since Convolutional Neural Networks (CNNs) [35] were first used by Long *et al.* [40] for semantic segmentation, they have become the state-of-the-art method for this problem. Most of the architectures are based on an encoder-decoder design such as [40, 52, 6]. Skip connections [52] and atrous / dilated convolutions [4, 68] help to preserve details in the segmentation and spatial pyramid pooling [15, 73, 5] aggregates information from different scales to exploit spatial context information.

Semi-supervised semantic segmentation makes use of additional unlabeled data during training. For that purpose, Souly *et al.* [60] and Hung *et al.* [23] utilize generative adversarial networks [18], where a generator is trained to predict real looking images while a discriminator simultaneously learns to distinguish real and generated samples. Souly *et al.* [60] use that concept to generate additional training samples, while Hung *et al.* [23] train the

discriminator based on the semantic segmentation probability maps. s4GAN [43] extends this idea by adding a multi-label classification mean teacher [61]. Another line of work [48, 12, 47] is based on consistency training, where perturbations are applied to unlabeled images or their intermediate features and a loss term enforces that the perturbations should not change the segmentation. While Ouali *et al.* [48] study perturbation of encoder features for consistency regularization, CutMix [12] mixes crops from the input image and their pseudo labels to generate additional training data, and ClassMix [47] uses pseudo label [36] class segments to build the mix mask. Our proposed DepthMix module is inspired by these methods but, in contrast, it also respects the structure of the scene when mixing samples. Commonly, several approaches [43, 12, 47, 11] include self training with pseudo-labels [36] and a mean teacher framework [61], which is extended by Feng *et al.* [11] with a class-balanced curriculum. Another related line of work is learning useful representations for semantic segmentation from self-supervised tasks such as tracking [64], context inpainting [50], colorization [34], depth estimation [26] (discussed in detail in Section 2.3), or optical flow prediction [37]. However, all of these approaches are outperformed by ImageNet pretraining and are, therefore, not relevant for semi-supervised semantic segmentation in practice.

2.2. Active Learning

Another approach to reduce the number of required annotations is active learning. It iteratively requests the most informative samples to be labeled. Two main directions for the selection heuristic can be differentiated. On the one side, uncertainty-based approaches select samples with a high uncertainty estimated based on, e.g., entropy [24, 55] or ensemble disagreement [56, 42]. However, this can be prone to querying outliers. On the other side, diversity-based approaches select samples, which most increase the diversity of the labeled set [44, 53, 59]. For semantic segmentation, active learning is typically based on uncertainty measures such as MC dropout [13, 67, 41], entropy [29, 65], or multi view consistency [58]. In addition to methods selecting whole images [19, 67, 65], several approaches apply a more fine-grained label request at region level [41, 29, 58] partly including also a label cost estimate [41, 29].

In contrast to these works, we perform unsupervised data selection for annotation, which does not require any human-in-the-loop annotation during the sample selection process. Even though unsupervised active learning has been studied in the past [69, 71, 45, 22, 57, 39], all of these methods are restricted to shallow models. Only [38] concurrently showed that unsupervised active learning can be applied to deep learning in the context of classification with low-dimensional inputs.

2.3. Improving Segmentation with SDE

Self-supervised depth estimation (SDE) aims to learn models for depth estimation with the geometric relations between the outputs. The problem has been approached using stereo image pairs [14, 16] and monocular videos [74]. In our work, monocular videos are also used as input. This line of research was pioneered by Zhou *et al.* [74], where they build a pose network to predict the transformation between two subsequent images, and use a photometric loss computed after a differentiable warping. The approach has been improved by many follow-up works [17, 8, 75].

The combination of semantic segmentation and SDE was studied in previous works with the goal of improving the depth estimation. While [51, 28, 7] learn both tasks jointly, [3, 20, 27] distill knowledge from a teacher semantic segmentation network to guide SDE. To further utilize coherence between semantic segmentation, [51, 7] have proposed additional loss terms that encourage spatial proximity between depth discontinuities and segmentation contours.

In contrast to these works, we do not aim to improve SDE but rather to improve semi-supervised semantic segmentation. The closest to our approach are the works of Jiang *et al.* [26] and Novosel *et al.* [46]. Jiang *et al.* [26] utilizes automatically computed relative depth based on optical flow as supervision to pretrain a neural network for semantic segmentation. While [26] mainly studies learning a useful representation complementary to ImageNet pretraining for transfer learning semantic segmentation, we study multi-task learning of SDE and semantic segmentation and show that combining SDE with ImageNet features can even further boost performance. Novosel *et al.* [46] improves the semantic segmentation performance by jointly learning *stereo* SDE and colorization. However, [46] focuses on the fully-supervised setting, while our work explicitly addresses the challenges of semi-supervised semantic segmentation by using the depth estimates to generate additional training data and an unsupervised data selection mechanism based on SDE. Also, in contrast to [46], we do not require calibrated stereo image pairs and suffice with easier to acquire image sequences. Another work supporting the usefulness of SDE for semantic segmentation from another viewpoint is [31] by Klingner *et al.* demonstrating an improved noise and attack robustness.

3. Methods

In this section, we present our three ways to improve the performance of semantic segmentation with self-supervised depth estimation (SDE). They focus on three different aspects of semantic segmentation, covering data selection for annotation, data augmentation, and multi-task learning. Given N images and K image sequences, both from the same domain, our first method, *Unsupervised Data Se-*

lection for Annotation, uses SDE learned on the K (unlabeled) sequences to select N_A images out of the N images for human annotation (see Alg. 1). Our second task, termed *DepthMix*, leverages the learned SDE to create geometrically-sound 'virtual' training samples from pairs of labeled images and their annotations (see Fig. 1). Our third method learns semantic segmentation with SDE as an auxiliary task under a multi-tasking framework (see Fig. 2). The learning is reinforced by a multi-task pretraining process combining SDE with image classification. We demonstrate the effectiveness of these three methods in both supervised setting and semi-supervised setting.

For SDE, we follow the method of Godard *et al.* [17], which we briefly introduce in the following. We first train a depth estimation network f_D to predict the depth of a target image and a pose estimation network f_T to estimate the camera motion from the target image and the source image. Depth and pose are used to produce a differentiable warping to transform the source image into the target image. The photometric error between the target image and multiple warped source frames is combined by a pixel-wise minimum. Besides, stationary pixels are masked out and an edge-aware depth smoothness term is applied resulting in the final self-supervised depth loss L_D . We refer to the original paper [17] for more details.

3.1. Unsupervised Data Selection for Annotation

In this section, we use SDE for selecting N_A samples out of a set of N unlabeled samples for human to create annotations for semantic segmentation. The selection is conducted progressively in multiple steps, similar to the standard active learning. However, our selection is fully automatic and does not require a human in the loop.

Let's denote by \mathcal{G} , \mathcal{G}_A and \mathcal{G}_U , the whole image set, the selected sub-set for annotation, and the un-selected sub-set. We have $\mathcal{G}_A = \emptyset$ and $\mathcal{G}_U = \mathcal{G}$ at the beginning. The selection is driven by two criteria: *diversity* and *uncertainty*. Diversity sampling encourages that selected images are diverse and cover different scenes. Uncertainty sampling favors adding unlabeled images that are near a decision boundary (with high uncertainties) in the model trained on the current \mathcal{G}_A . For uncertainty sampling, we need to train and update the model with \mathcal{G}_A . It is inefficient to repeat this every time a new image is added. For the sake of efficiency, we divide the selection into T steps and only train the model T times. In each step t , n_t images will be selected and moved from \mathcal{G}_U to \mathcal{G}_A , so we have $\sum_{t=1}^T n_t = N_A$. After each step t , a model is trained on \mathcal{G}_A and evaluated on \mathcal{G}_U to get updated uncertainties for step $t + 1$.

Diversity Sampling: To ensure that the chosen annotated samples are diverse enough to represent the entire dataset well, we use an iterative farthest point sampling based on the distance over features Φ^{SDE} computed by the SDE net-

Algorithm 1: Unsupervised Data Selection

- 1: $t = 1$
 - 2: $i \leftarrow \text{uniform}(1, N)$
 - 3: $\mathcal{G}_A = \{I_i\}$ and $\mathcal{G}_U = \mathcal{G}_U \setminus \{I_i\}$
 - 4: **for** $k = 2$ **to** N_A **do**
 - 5: **if** $k == \sum_{l=1}^t n_l$ **then**
 - 6: Train depth student Φ_{SIDE} on the current \mathcal{G}_A
 - 7: Calculate $E(i) \forall I_i \in \mathcal{G}_U$
 - 8: $t = t + 1$
 - 9: **end if**
 - 10: **if** $t == 1$ **then**
 - 11: Obtain index i according to Eq. 2
 - 12: **else**
 - 13: Obtain index i according to Eq. 4
 - 14: **end if**
 - 15: $\mathcal{G}_A = \mathcal{G}_A \cup \{I_i\}$ and $\mathcal{G}_U = \mathcal{G}_U \setminus \{I_i\}$
 - 16: **end for**
-

work. For the desired layer L , the spatial resolution is reduced by average pooling and the L2 distance is computed for each sample pair in \mathcal{G} .

At step t , for each of the n_t samples, we choose the one in \mathcal{G}_U with the largest distance to the current annotation set \mathcal{G}_A . The set of selected samples \mathcal{G}_A is iteratively extended by moving one image at a time from \mathcal{G}_U to \mathcal{G}_A until the n_t images are collected:

$$\mathcal{G}_U = \mathcal{G}_U \setminus \{I_i\} \text{ and } \mathcal{G}_A = \mathcal{G}_A \cup \{I_i\}, \quad (1)$$

$$i = \arg \max_{I_i \in \mathcal{G}_U} \min_{I_j \in \mathcal{G}_A} \|\Phi_i^{\text{SDE}} - \Phi_j^{\text{SDE}}\|_2. \quad (2)$$

Uncertainty Sampling: While Diversity Sampling is able to select diverse new samples, it is unaware of the uncertainties of a semantic segmentation model over these samples. Uncertainty Sampling aims to select difficult samples, *i.e.*, samples in \mathcal{G}_U that the model trained on the current \mathcal{G}_A cannot handle well. In order to train this model, active learning typically uses a human-in-the-loop strategy to add annotations for selected samples. In this work, in order to make the method flexible and efficient, we use a proxy task based on self-supervised annotations, which can run automatically. Since our target task is single-image semantic segmentation, we choose to use single-image depth estimation (SIDE) as the proxy task. Importantly, due to our SDE framework, pseudo depth labels are available for \mathcal{G} . Using these pseudo-labels, we train a SIDE method on \mathcal{G}_A and measure the uncertainty of its depth predictions on \mathcal{G}_U . Due to the high correlation of single-image semantic segmentation and SIDE, the generated uncertainties are informative and can be used to guide our sampling procedure. Note that the SDE method is trained on a much larger unlabeled dataset, *i.e.*, the K image sequences, and can provide good guidance for the SIDE method.

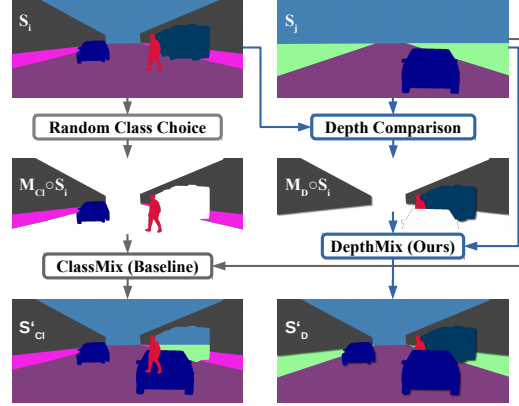


Figure 1. Concept of the proposed DepthMix augmentation and its baseline ClassMix. By utilizing SDE, DepthMix avoids geometric artifacts.

In particular, the uncertainty is signaled by the disparity error between the student network f_{SIDE} and the teacher network f_{SDE} in the log-scale space under L1 distance:

$$E(i) = \|\log(1 + f_{\text{SDE}}(I_i)) - \log(1 + f_{\text{SIDE}}(I_i))\|_1. \quad (3)$$

This criterion can be added into Eq. 2 to select samples with higher uncertainties as well for the dataset update in Eq. 1:

$$i = \arg \max_{I_i \in \mathcal{G}_U} \min_{I_j \in \mathcal{G}_A} \|\Phi_i^{\text{SDE}} - \Phi_j^{\text{SDE}}\|_2 + \lambda_E E(i), \quad (4)$$

where λ_E is a parameter to balance the contribution of the two terms. When n_t images have been selected according to Eq. 1 and Eq. 4 at step t , a new SIDE model will be trained on the current \mathcal{G}_A in order to continue further. As presented previously, our selection proceeds progressively in T steps until we collect all N_A images. The algorithm of this selection is summarized in Alg. 1.

3.2. DepthMix Data Augmentation

Inspired by the recent success of data augmentation approaches that mixup pairs of images and their (pseudo) labels to generate more training samples for semantic segmentation [70, 12, 47], we propose an algorithm, termed DepthMix, to utilize self-supervised depth estimates to maintain the integrity of the scene structure during mixing.

Given two images I_i and I_j of the same size, we would like to copy some regions from I_i and paste them directly into I_j to get a virtual sample I' . The copied regions are indicated by a mask M , which is a binary image of the same size as the two images. The image creation is done as

$$I' = M \odot I_i + (1 - M) \odot I_j, \quad (5)$$

where \odot denotes the element-wise product. The label maps of the two images S_i and S_j are mixed up with the same

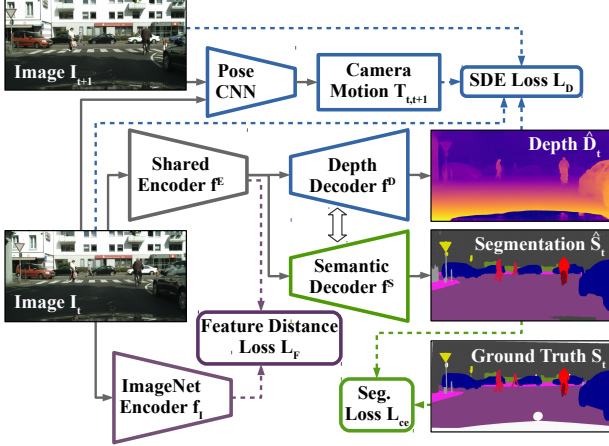


Figure 2. Architecture for learning semantic segmentation with SDE as auxiliary task. Note that the architecture also accepts data with single images or without segmentation ground truth. In that case the SDE or the cross-entropy loss, respectively, are disabled.

mask M to generate S' . The mixing can be applied to labeled data as well as to unlabeled data using human ground truths or pseudo-labels, respectively. Existing methods generate this mask M in different ways, *e.g.*, randomly sampled rectangular regions [70, 12] or randomly selected object segments [47]. In those methods, the structure of the scene is not considered and fore- and background are not distinguished. We find images synthesized by these methods often violate the geometric relationships between objects. For instance, a distant object can be copied onto a close-range object or only unoccluded parts of mid-range objects are copied onto the other image. Imagine how strange it is to see a pedestrian standing on top of a car or to see sky through a hole in a building (just as shown in Fig. 1 left).

Our DepthMix is designed to mitigate this issue. It uses the estimated depth \hat{D}_i and \hat{D}_j of the two images to generate the mix mask M that respects the notion of geometry. It is implemented by selecting only pixels from I_i whose depth values are smaller than the depth values of the pixels at the same locations in I_j :

$$M(a, b) = \begin{cases} 1 & \text{if } \hat{D}_i(a, b) < \hat{D}_j(a, b) + \epsilon \\ 0 & \text{otherwise} \end{cases} \quad (6)$$

where a and b are pixel indices, and ϵ is a small value to avoid conflicts of objects that are naturally at the same depth plane such as road or sky. By using this M , DepthMix respects the depth of objects in both images, such that only closer objects can occlude further-away objects and not the other way around. We illustrate this advantage of DepthMix with an example in Fig. 1.

3.3. Semi-Supervised Semantic Segmentation

In this section, we train a semantic segmentation model utilizing the labeled image dataset \mathcal{G}_A , the unlabeled image

dataset \mathcal{G}_U , and K unlabeled image sequences. We first discuss how to exploit SDE on the image sequences to improve our semantic segmentation. We then show how to use \mathcal{G}_U to further improve the performance.

Learning with Auxiliary Tasks: For learning semantic segmentation and SDE jointly, we use a network with shared encoder f_θ^E and a separate depth f_θ^D and segmentation decoder f_θ^S (see Fig. 2). The depth branch is trained using the SDE loss L_D and the segmentation branch $g_\theta^S = f_\theta^S \circ f_\theta^E$ is trained using the pixel-wise cross-entropy L_{ce} .

In order to initialize the pose estimation network and the depth decoder properly, the architecture is first trained on K unlabeled image sequences for SDE. As a common practice, we initialize the encoder with ImageNet weights as they provide useful semantic features learned during image classification. To avoid forgetting these features during the SDE pretraining, we utilize a feature distance loss between the current bottleneck features f_θ^E and the bottleneck features of the encoder with ImageNet weights f_I^E :

$$L_F = \|f_\theta^E - f_I^E\|_2. \quad (7)$$

The loss for the depth pretraining is the weighted sum of the SDE loss and the ImageNet feature distance loss:

$$L_P = L_D + \lambda_F L_F. \quad (8)$$

To additionally incorporate transfer learning from depth estimation to semantic segmentation in our architecture, the weights of f_θ^D are used to initialize f_θ^S .

Learning with Unlabeled Images: In order to further utilize the unlabeled dataset \mathcal{G}_U , we generate pseudo-labels by following a common practice in semi-supervised learning [1, 63, 12, 47] using the mean teacher algorithm [61]. For that purpose, an exponential moving average is applied to the weights of the semantic segmentation model g_θ^S to obtain the weights of the mean teacher θ_T :

$$\theta'_T = \alpha \theta_T + (1 - \alpha) \theta. \quad (9)$$

To generate the pseudo-labels, an argmax over the classes C is applied to the prediction of the mean teacher.

$$S_U = \arg \max_{c \in C} (g_{\theta_T}^S(I_U)). \quad (10)$$

The mean teacher can be considered as a temporal ensemble, resulting in stable predictions for the pseudo-labels, while the argmax ensures confident predictions.

For the semi-supervised setting, the segmentation network is trained with labeled samples (I_A, S_A) and pseudo-labeled samples (I_U, S_U) :

$$L_{SSL} = L_{ce}(g_\theta^S(I_A), S_A) + \lambda_P(S_U) L_{ce}(g_\theta^S(I_U), S_U) \quad (11)$$

$\lambda_P(S_U)$ is chosen to reflect the quality of the pseudo-label represented by the fraction of pixels exceeding a threshold τ for predicted probability of the most confident class $\max_{c \in C}(g_{\theta_T}^S(I_U))$, as suggested in [47]. We incorporate DepthMix samples (I' , S'), which are obtained from the combined labeled and pseudo-labeled data pool $I_i, I_j \in \mathcal{G}_A \cup \mathcal{G}_U$ (see Eq. 5), into Eq. 11 to replace the unlabeled samples (S_U , L_U). Our semi-supervised learning is now changed to:

$$L_{SSL} = L_{ce}(g_{\theta}^S(I_A), S_A) + \lambda_P(S')L_{ce}(g_{\theta}^S(I'), S'). \quad (12)$$

4. Experiments

4.1. Implementation Details

Dataset: We evaluate our method on the Cityscapes dataset [9], which consists of 2975 training and 500 validation images with semantic segmentation labels from European street scenes. We downsample the images to 1024×512 pixels. Besides, random cropping to a size of 512×512 and random horizontal flipping are used in the training. Importantly, Cityscapes provides 20 unlabeled frames before and 10 after the labeled image, which are used for the self-supervised depth estimation (SDE) training. During the semi-supervised semantic segmentation training, only the originally 2975 labeled training images are used. They are randomly split into a labeled and an unlabeled subset.

Network Architecture: Our network consists of a shared ResNet101 [21] encoder with output stride 16, and one decoder for segmentation and one for SDE. The decoder consists of an ASPP [5] block to aggregate features from multiple scales and another four upsampling blocks with skip connections [52]. For SDE, the upsampling blocks have a disparity side output at the respective scale. For effective multi-task learning, we additionally follow PAD-Net [66] and deploy an attention guided distillation module after the third decoder block. It serves the purpose of exchanging useful features between segmentation and depth estimation. In experiments without multi-task learning, only the semantic segmentation decoder is used for efficiency.

Training: For the SDE pretraining, the depth and pose network are trained using Adam [30] with a batch size of 4 and an initial learning rate of 1×10^{-4} , which is decreased after 160k iterations by a factor of 10. The SDE loss is calculated on four scales with the three subsequent images. During the first 300k iterations, only the depth decoder and the pose network are trained. Afterwards, the depth encoder is fine-tuned with an ImageNet feature distance $\lambda_F = 1 \times 10^{-2}$ for another 50k iterations. All encoder networks are initialized with ImageNet weights, either before depth pretraining or before semantic segmentation if depth pretraining is disabled for an experiment.

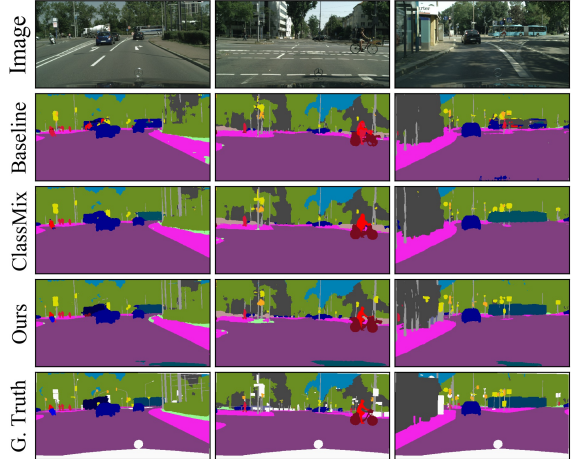


Figure 3. Example semantic segmentations of our method (including data selection) for 100 labeled samples in comparison with ClassMix [47] and the baseline.

For the multi-task setting, we train the network using SGD with a learning rate of 1×10^{-3} for the encoder and depth decoder, 1×10^{-2} for the segmentation decoder, and 1×10^{-6} for the pose network. The learning rate is reduced by 10 after 30k iterations and trained for another 10k iterations. A momentum of 0.9, a weight decay of 5×10^{-4} , and a gradient norm clipping to 10 are used. The loss for segmentation and SDE are weighted equally. The mean teacher has $\alpha = 0.99$ and within an iteration, the network is trained on a labeled, unaugmented and a (un)labeled, augmented batch with size 2, respectively. The augmented batch uses DepthMix with $\epsilon = 0.03$ (or another mixing algorithm), color jitter, and Gaussian blur.

Data Selection for Annotation: In the data selection experiment, we use a slimmed network architecture with a ResNet50 encoder and fewer decoder channels for f_{SIDE} , which is trained using Adam with 1×10^{-4} learning rate and polynomial decay with exponent 0.9 for faster convergence. Experiments show that data selected by a smaller network is able to bring benefits to larger networks as well. For calculating the depth feature diversity, we use the output of the second depth decoder block after SDE pretraining, which is downsampled by average pooling to a size of 8×4 pixels and the feature channels are normalized to zero-mean unit-variance over the dataset. The student depth error is weighted by $\lambda_E = 10$. The number of the selected samples ($\sum_{l=1}^t n_l$) is iteratively increased to 25, 50, 100, 200, 372, and 744. For each subset, a student depth network is trained from scratch for 4k, 8k, 12k, 16k, and 20k iterations, respectively, to calculate the student depth error and select the samples for the next subset.

Table 1. Performance on the Cityscapes validation set (mIoU in %, standard deviation over 3 random seeds).

Labeled Samples	1/30 (100)	1/8 (372)	1/4 (744)	Full (2975)
Baseline [23]	-	55.50 ↘	59.90 ↘	66.40 ↘
Adversarial [23]	-	58.80 +3.30	62.30 +2.40	-
Baseline [43]	-	56.20 ↘	60.20 ↘	66.00
s4GAN [43]	-	59.30 +3.10	61.90 +1.70	65.80 -0.20
Baseline [12]	44.41 ±1.11 ↘	55.25 ±0.66 ↘	60.57 ±1.13 ↘	67.53 ±0.35 ↘
CutMix [12]	51.20 ±2.29 +6.79	60.34 ±1.24 +5.09	63.87 ±0.71 +3.30	67.68 ±0.37 +0.15
Baseline [11]	45.50 ↘	56.70 ↘	61.10 ↘	66.90
DST-CBC [11]	48.70 +3.20	60.50 +3.80	64.40 +3.30	-
Baseline [47]	43.84 ±0.71 ↘	54.84 ±1.14 ↘	60.08 ±0.62 ↘	66.19 ±0.11
ClassMix [47]	54.07 ±1.61 +10.23	61.35 ±0.62 +6.51	63.63 ±0.33 +3.55	-
Baseline [26]	-	48.8 ↘	52.7 ↘	58.8 ↘
Jiang et al. [26] ¹	-	41.7 -7.1	47.2 -5.5	55.0 -3.8
Baseline [46]	-	-	-	61
Novosel et al. [46]	-	-	-	64 +3
Baseline	48.75 ±1.61 ↘	59.14 ±1.02 ↘	63.46 ±0.38 ↘	67.77 ±0.13 ↘
ClassMix ²	56.82 ±1.65 +8.07	63.86 ±0.41 +4.72	65.57 ±0.71 +2.11	-
Ours	58.40 ±1.36 +9.65	66.66 ±1.05 +7.52	68.43 ±0.06 +4.98	71.16 ±0.16 +3.40
Ours (+Data Selection)	63.29 ±0.59 +14.54	68.98 ±0.37 +9.84	70.61 ±0.30 +7.15	-

4.2. Semi-Supervised Semantic Segmentation

First, we compare our approach with several semi-supervised learning approaches, to facilitate the comparison with state-of-the-arts. We summarize the results in Tab. 1. The performance (mIoU in %) of the semi-supervised methods and their baselines (only trained on the labeled dataset) are shown for different number of labeled samples. As the performance of the baselines differ, there are columns showing the absolute improvement for better comparability. As our baseline utilizes a more capable network architecture due to the U-Net decoder with ASPP as opposed to a DeepLabv2 decoder used by most previous works, we also reimplemented the state-of-the-art method, ClassMix [47] for reference. We test it with the identical architecture and training parameters to ensure a direct comparison.

As shown in Tab. 1, our method outperforms all other approaches on each labeled subset size for both the absolute performance as well as the improvement to the baseline. The only exception is the absolute improvement of the original results of ClassMix for the case of 100 labeled samples. However, if we consider ClassMix trained in our setting, our method outperforms it also in this particular case. This can be explained by the considerably higher baseline performance in our setting, which increases the difficulty to achieve an high improvement. Note that our method also significantly improves over the related SDE representation learning work by [26]. Adding data selection even further increases the performance by a significant margin, so that using 1/8 of the training labels, it even outperforms

the baseline with the completely annotated dataset.

The adequacy of our approach is also reflected in the example predictions in Fig. 3. We can observe that the contours of classes are more precise. Moreover, difficult objects such as bus, train, motorbike, or truck can be better distinguished. This observation is also quantitatively confirmed by the class-wise IoU improvement shown in Fig. 4.

4.3. Ablation Study

Next, we analyze the individual contribution of each component of the proposed method. For this purpose, we test several ablated versions of our model for both the cases of 372 and 2975 labeled samples. We summarize the results in Tab. 2. The overall performance improvement can mostly be attributed to the SDE pretraining, the DepthMix augmentation, the unsupervised data selection, and the mean teacher. In particular, transfer learning, improves the performance by 1.66 percent point, the mean teacher by another 2.98 percent point, DepthMix by another 2.41 percent point, multi-task learning by another 0.47 percent point, and data selection by another 2.32 percent point for the case of 372 labeled samples, which shows the effectiveness of the proposed modules. For the fully annotated training set with 2975 samples, we can still observe a significant improvement of 1.71 percent point by using SDE pretraining, probably as it learns useful features from the full unlabeled

¹Jiang et al. studies the representation learning aspect of SDE. The performance decrease is caused by forgoing ImageNet pretraining in their method. The listed results were extracted from their Fig. 3b.

² Results of the reimplemention in our experiment setting.

Table 2. Ablation of the architecture components (D-P: SDE Transfer Learning (Pretraining), D-M SDE Transfer and Multi-Task Learning, F: ImageNet Feature Distance Loss, T: Mean Teacher, X-C: Mix Class, X-D: Mix Depth, L: Additionally mix labeled samples with their ground truth, S - Data Selection). mIoU in %, standard deviation over 3 seeds.

D	F	T	X	L	S	372 Samples	2975 Samples
						59.14 \pm 1.02 \curvearrowright	67.77 \pm 0.13 \curvearrowright
P						60.46 \pm 0.64 +1.31	69.00 \pm 0.70 +1.23
P	✓					60.80 \pm 0.69 +1.66	69.47 \pm 0.38 +1.71
M	✓					61.25 \pm 0.55 +2.10	69.76 \pm 0.39 +1.99
		✓				62.39 \pm 0.86 +3.24	-
		✓	C			63.86 \pm 0.41 +4.72	-
P	✓	✓				63.78 \pm 0.49 +4.64	-
P	✓	✓	C			64.68 \pm 0.81 +5.54	-
P	✓	✓	C	✓		64.83 \pm 0.57 +5.69	70.84 \pm 0.09 +3.08
P	✓	✓	D	✓		66.19 \pm 1.06 +7.05	71.10 \pm 0.33 +3.33
M	✓	✓	D	✓		66.66 \pm 1.05 +7.52	71.16 \pm 0.16 +3.40
P	✓	✓	D	✓	✓	68.73 \pm 0.74 +9.59	-
M	✓	✓	D	✓	✓	68.98 \pm 0.37 +9.84	-

set of video sequences. Also, DepthMix results in another performance boost of 1.63 percent point. Only multi-task learning, does not improve the performance by a significant margin compared to transfer learning for 2975 samples.

Furthermore, we compare DepthMix in more detail with ClassMix. For a fair comparison, we transfer ClassMix to our setting, which includes depth pretraining and additionally mixing labeled samples with their ground truth. This already results in an improvement from 63.86% mIoU to 64.83% mIoU, again demonstrating the effectiveness of depth pretraining. But it also can be seen that DepthMix still outperforms the improved ClassMix by 1.36 percent point for the setting of 372 annotated samples, which shows the effect of the geometry aware augmentation.

For more insights into possible reasons of these improvements, we visualize the improvement of the architecture components over the baseline for each class separately in Fig. 4. It can be seen that depth pretraining (DP) improves mostly the classes wall, fence, pole, traffic light, and truck, which is possibly due to their characteristic depth profile learned during SDE. For example, a good depth estimation performance, requires correctly segmenting poles or traffic signs as missing them can cause large depth errors. This can qualitatively also be seen in Fig. 3. The only class with a lower performance than the baseline is motorcycle, possibly due to the fact that the depth features were not useful for distinguishing motorcycle and bicycle as this is not relevant for depth estimation. DepthMix (XD) further improves the performance of wall, fence, and truck but also of train and motorcycle. This might be caused by the fact the DepthMix presents those rather difficult objects in other context,

Table 3. Comparison of data selection methods (DS: Diversity Sampling base on depth features, US: Uncertainty Sampling based on depth student error). mIoU in %, std. dev. over 3 seeds.

# Labeled	1/30 (100)	1/8 (372)	1/4 (744)
Random	48.75 \pm 1.61	59.14 \pm 1.02	63.46 \pm 0.38
Entropy	53.63 \pm 0.77	63.51 \pm 0.68	66.18 \pm 0.50
Ours (DS)	52.83 \pm 0.23	63.34 \pm 0.26	67.20 \pm 0.28
Ours (DS+US)	54.72 \pm 0.39	64.53 \pm 0.19	67.67 \pm 0.41
All Labels	67.77 \pm 0.13		

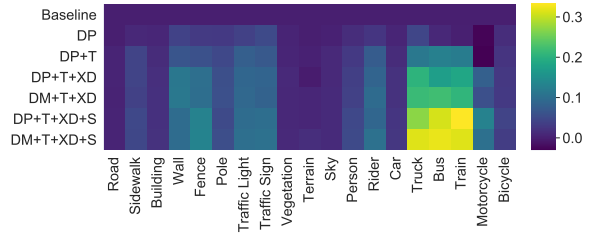


Figure 4. Improvement of the class-wise IoU over the baseline performance for 372 labeled samples (DP: SDE Pretraining, DM: SDE Multi-Task Learning, T: Mean Teacher, XD: DepthMix, S: Data Selection).

which might help the network to generalize better.

4.4. Unsupervised Data Selection for Annotation

Finally, we evaluate the proposed unsupervised data selection. Tab. 3 shows a comparison of our method with a baseline and a competing method. The baseline selects the labeled samples randomly, while the second, strong competitor uses active learning and iteratively chooses the samples with the highest segmentation entropy, which, in contrast to our methods, requires a human in the loop to create the semantic labels for already-selected images. It can be seen that our method with the Diversity Sampling (DS) and the Uncertainty Sampling (US) outperforms both comparison methods by a noticeable margin, demonstrating the effectiveness of ensuring diversity and exploiting difficult samples based on depth. It also supports the assumption that single-image depth estimation and single-image semantic segmentation are correlated in terms of sample difficulties. The class-wise analysis (see the last two rows of Fig. 4) shows that data selection significantly improves the performance for truck, bus, and train, which are usually difficult to distinguish in a semi-supervised setting. We would like to note that our unlabeled data selection method can be applied to any semantic segmentation method.

5. Conclusion

In this work, we have studied how self-supervised depth estimation (SDE) can be utilized to improve semantic seg-

mentation, in both semi-supervised and fully-supervised setting. We introduced three effective strategies capable of leveraging the knowledge learned from SDE. First, we show that the SDE feature representation can be transferred to semantic segmentation, by means of SDE pretraining and joint learning of segmentation and depth. Second, we demonstrate that the proposed DepthMix strategy outperforms related mixing strategies by avoiding inconsistent geometry of the generated images. Third, we present an unsupervised data selection for annotation algorithm based on SDE, which does not require human-in-the-loop annotations. We validate the benefits of the three components by extensive experiments on Cityscapes, where we demonstrate significant gains over the baselines and competing methods. By using SDE, our approach achieves state-of-the-art performance, suggesting that SDE can be a valuable self-supervision for semantic segmentation.

Acknowledgements: This work is funded by Toyota Motor Europe via the research project TRACE-Zurich and also by a research project from armasuisse.

References

- [1] David Berthelot, Nicholas Carlini, Ian Goodfellow, Nicolas Papernot, Avital Oliver, and Colin A Raffel. Mixmatch: A holistic approach to semi-supervised learning. In *Adv. Neural Inform. Process. Syst.*, pages 5049–5059, 2019. [5](#)
- [2] Gabriel J Brostow, Julien Fauqueur, and Roberto Cipolla. Semantic object classes in video: A high-definition ground truth database. *Pattern Recognition Letters*, pages 88–97, 2009. [12](#)
- [3] Vincent Casser, Soeren Pirk, Reza Mahjourian, and Anelia Angelova. Depth prediction without the sensors: Leveraging structure for unsupervised learning from monocular videos. In *AAAI Conf. Artif. Intell.*, pages 8001–8008, 2019. [3](#), [13](#)
- [4] Liang-Chieh Chen, George Papandreou, Iasonas Kokkinos, Kevin Murphy, and Alan L Yuille. Semantic image segmentation with deep convolutional nets and fully connected crfs. *arXiv preprint arXiv:1412.7062*, 2014. [2](#)
- [5] Liang-Chieh Chen, George Papandreou, Iasonas Kokkinos, Kevin Murphy, and Alan L Yuille. Deeplab: Semantic image segmentation with deep convolutional nets, atrous convolution, and fully connected crfs. *IEEE Trans. Pattern Anal. Mach. Intell.*, pages 834–848, 2017. [1](#), [2](#), [6](#), [12](#)
- [6] Liang-Chieh Chen, Yukun Zhu, George Papandreou, Florian Schroff, and Hartwig Adam. Encoder-decoder with atrous separable convolution for semantic image segmentation. In *Eur. Conf. Comput. Vis.*, pages 801–818, 2018. [2](#)
- [7] Po-Yi Chen, Alexander H Liu, Yen-Cheng Liu, and Yu-Chiang Frank Wang. Towards scene understanding: Unsupervised monocular depth estimation with semantic-aware representation. In *IEEE Conf. Comput. Vis. Pattern Recog.*, pages 2624–2632, 2019. [3](#)
- [8] Yuhua Chen, Cordelia Schmid, and Cristian Sminchisescu. Self-supervised learning with geometric constraints in monocular video: Connecting flow, depth, and camera. In *Int. Conf. Comput. Vis.*, pages 7063–7072, 2019. [3](#)
- [9] Marius Cordts, Mohamed Omran, Sebastian Ramos, Timo Rehfeld, Markus Enzweiler, Rodrigo Benenson, Uwe Franke, Stefan Roth, and Bernt Schiele. The cityscapes dataset for semantic urban scene understanding. In *IEEE Conf. Comput. Vis. Pattern Recog.*, pages 3213–3223, 2016. [1](#), [2](#), [6](#)
- [10] Qi Dai, Vaishakh Patil, Simon Hecker, Dengxin Dai, Luc Van Gool, and Konrad Schindler. Self-supervised object motion and depth estimation from video. In *IEEE Conf. Comput. Vis. Pattern Recog. Workshops*, pages 1004–1005, 2020. [13](#)
- [11] Zhengyang Feng, Qianyu Zhou, Guangliang Cheng, Xin Tan, Jianping Shi, and Lizhuang Ma. Semi-supervised semantic segmentation via dynamic self-training and class-balanced curriculum. *arXiv preprint arXiv:2004.08514*, 2020. [2](#), [7](#)
- [12] Geoff French, Timo Aila, Samuli Laine, Michal Mackiewicz, and Graham Finlayson. Consistency regularization and cutmix for semi-supervised semantic segmentation. *arXiv preprint arXiv:1906.01916*, 2019. [2](#), [4](#), [5](#), [7](#)
- [13] Yarin Gal and Zoubin Ghahramani. Dropout as a bayesian approximation: Representing model uncertainty in deep learning. In *Int. Conf. Mach. Learning*, pages 1050–1059, 2016. [2](#)
- [14] Ravi Garg, Vijay Kumar BG, Gustavo Carneiro, and Ian Reid. Unsupervised cnn for single view depth estimation: Geometry to the rescue. In *Eur. Conf. Comput. Vis.*, pages 740–756, 2016. [3](#)
- [15] Golnaz Ghiasi and Charless C Fowlkes. Laplacian pyramid reconstruction and refinement for semantic segmentation. In *Eur. Conf. Comput. Vis.*, pages 519–534, 2016. [2](#)
- [16] Clément Godard, Oisín Mac Aodha, and Gabriel J Brostow. Unsupervised monocular depth estimation with left-right consistency. In *IEEE Conf. Comput. Vis. Pattern Recog.*, pages 270–279, 2017. [1](#), [3](#)
- [17] Clément Godard, Oisín Mac Aodha, Michael Firman, and Gabriel J Brostow. Digging into self-supervised monocular depth estimation. In *Int. Conf. Comput. Vis.*, pages 3828–3838, 2019. [1](#), [3](#), [12](#)
- [18] Ian Goodfellow, Jean Pouget-Abadie, Mehdi Mirza, Bing Xu, David Warde-Farley, Sherjil Ozair, Aaron Courville, and Yoshua Bengio. Generative adversarial nets. In *Adv. Neural Inform. Process. Syst.*, pages 2672–2680, 2014. [2](#)
- [19] Marc Gorriz, Axel Carlier, Emmanuel Faure, and Xavier Giro-i Nieto. Cost-effective active learning for melanoma segmentation. *arXiv preprint arXiv:1711.09168*, 2017. [2](#)
- [20] Vitor Guizilini, Rui Hou, Jie Li, Rares Ambrus, and Adrien Gaidon. Semantically-guided representation learning for self-supervised monocular depth. *arXiv preprint arXiv:2002.12319*, 2020. [3](#)
- [21] Kaiming He, Xiangyu Zhang, Shaoqing Ren, and Jian Sun. Deep residual learning for image recognition. In *IEEE Conf. Comput. Vis. Pattern Recog.*, pages 770–778, 2016. [6](#)
- [22] Yao Hu, Debing Zhang, Zhongming Jin, Deng Cai, and Xiaofei He. Active learning via neighborhood reconstruction. In *Int. Joint Conf. Artif. Intell.*, pages 1415–1421, 2013. [2](#)

- [23] Wei-Chih Hung, Yi-Hsuan Tsai, Yan-Ting Liou, Yen-Yu Lin, and Ming-Hsuan Yang. Adversarial learning for semi-supervised semantic segmentation. *arXiv preprint arXiv:1802.07934*, 2018. [2](#), [7](#)
- [24] Rebecca Hwa. Sample selection for statistical parsing. *Computational linguistics*, pages 253–276, 2004. [2](#)
- [25] Sergey Ioffe and Christian Szegedy. Batch normalization: Accelerating deep network training by reducing internal covariate shift. *arXiv preprint arXiv:1502.03167*, 2015. [12](#)
- [26] Huaizu Jiang, Gustav Larsson, Michael Maire Greg Shakhnarovich, and Erik Learned-Miller. Self-supervised relative depth learning for urban scene understanding. In *Eur. Conf. Comput. Vis.*, pages 19–35, 2018. [2](#), [3](#), [7](#)
- [27] Huaizu Jiang, Deqing Sun, Varun Jampani, Zhaoyang Lv, Erik Learned-Miller, and Jan Kautz. Sense: A shared encoder network for scene-flow estimation. In *Int. Conf. Comput. Vis.*, pages 3195–3204, 2019. [3](#)
- [28] Jianbo Jiao, Ying Cao, Yibing Song, and Rynson Lau. Look deeper into depth: Monocular depth estimation with semantic booster and attention-driven loss. In *Eur. Conf. Comput. Vis.*, pages 53–69, 2018. [3](#)
- [29] Tejaswi Kasarla, Gattigorla Nagendar, Guruprasad M Hegde, Vineeth Balasubramanian, and CV Jawahar. Region-based active learning for efficient labeling in semantic segmentation. In *IEEE Winter Conf. Appl. of Comput. Vis.*, pages 1109–1117, 2019. [2](#)
- [30] Diederik P Kingma and Jimmy Ba. Adam: A method for stochastic optimization. *arXiv preprint arXiv:1412.6980*, 2014. [6](#)
- [31] Marvin Klingner, Andreas Bar, and Tim Fingscheidt. Improved noise and attack robustness for semantic segmentation by using multi-task training with self-supervised depth estimation. In *IEEE Conf. Comput. Vis. Pattern Recog. Workshops*, pages 320–321, 2020. [3](#)
- [32] Marvin Klingner, Jan-Aike Termöhlen, Jonas Mikolajczyk, and Tim Fingscheidt. Self-supervised monocular depth estimation: Solving the dynamic object problem by semantic guidance. *arXiv preprint arXiv:2007.06936*, 2020. [13](#)
- [33] Iro Laina, Christian Rupprecht, Vasileios Belagiannis, Federico Tombari, and Nassir Navab. Deeper depth prediction with fully convolutional residual networks. In *Int. Conf. 3D Vision*, pages 239–248, 2016. [12](#)
- [34] Gustav Larsson, Michael Maire, and Gregory Shakhnarovich. Colorization as a proxy task for visual understanding. In *IEEE Conf. Comput. Vis. Pattern Recog.*, pages 6874–6883, 2017. [2](#)
- [35] Yann LeCun, Léon Bottou, Yoshua Bengio, and Patrick Haffner. Gradient-based learning applied to document recognition. *Proceedings of the IEEE*, pages 2278–2324, 1998. [1](#), [2](#)
- [36] Dong-Hyun Lee. Pseudo-label: The simple and efficient semi-supervised learning method for deep neural networks. In *Int. Conf. Mach. Learning*, 2013. [2](#)
- [37] Seokju Lee, Junsik Kim, Tae-Hyun Oh, Yongseop Jeong, Donggeun Yoo, Stephen Lin, and In So Kweon. Visuomotor understanding for representation learning of driving scenes. *arXiv preprint arXiv:1909.06979*, 2019. [2](#)
- [38] Changsheng Li, Handong Ma, Zhao Kang, Ye Yuan, Xiao-Yu Zhang, and Guoren Wang. On deep unsupervised active learning. *Int. Joint Conf. Artif. Intell.*, 2020. [2](#)
- [39] Changsheng Li, Xiangfeng Wang, Weishan Dong, Junchi Yan, Qingshan Liu, and Hongyuan Zha. Joint active learning with feature selection via cur matrix decomposition. *IEEE Trans. Pattern Anal. Mach. Intell.*, pages 1382–1396, 2018. [2](#)
- [40] Jonathan Long, Evan Shelhamer, and Trevor Darrell. Fully convolutional networks for semantic segmentation. In *IEEE Conf. Comput. Vis. Pattern Recog.*, pages 3431–3440, 2015. [1](#), [2](#)
- [41] Radek Mackowiak, Philip Lenz, Omair Ghori, Ferran Diego, Oliver Lange, and Carsten Rother. Cereals-cost-effective region-based active learning for semantic segmentation. *arXiv preprint arXiv:1810.09726*, 2018. [2](#)
- [42] Andrew Kachites McCallumzy and Kamal Nigamy. Employing em and pool-based active learning for text classification. In *Int. Conf. Mach. Learning*, pages 359–367, 1998. [2](#)
- [43] Sudhanshu Mittal, Maxim Tatarchenko, and Thomas Brox. Semi-supervised semantic segmentation with high-and low-level consistency. *IEEE Trans. Pattern Anal. Mach. Intell.*, 2019. [2](#), [7](#)
- [44] Hieu T Nguyen and Arnold Smeulders. Active learning using pre-clustering. In *Int. Conf. Mach. Learning*, page 79, 2004. [2](#)
- [45] Feiping Nie, Hua Wang, Heng Huang, and Chris Ding. Early active learning via robust representation and structured sparsity. In *Int. Joint Conf. Artif. Intell.*, 2013. [2](#)
- [46] Jelena Novosel, Prashanth Viswanath, and Bruno Arsenali. Boosting semantic segmentation with multi-task self-supervised learning for autonomous driving applications. In *Int. Conf. Comput. Vis. Workshops*, 2019. [3](#), [7](#)
- [47] Viktor Olsson, Wilhelm Tranheden, Juliano Pinto, and Lennart Svensson. Classmix: Segmentation-based data augmentation for semi-supervised learning. *arXiv preprint arXiv:2007.07936*, 2020. [1](#), [2](#), [4](#), [5](#), [6](#), [7](#), [13](#)
- [48] Yassine Ouali, Céline Hudelot, and Myriam Tami. Semi-supervised semantic segmentation with cross-consistency training. *arXiv preprint arXiv:2003.09005*, 2020. [2](#)
- [49] Sinno Jialin Pan and Qiang Yang. A survey on transfer learning. *IEEE Transactions on Knowledge and Data Engineering*, pages 1345–1359, 2009. [1](#)
- [50] Deepak Pathak, Philipp Krahenbuhl, Jeff Donahue, Trevor Darrell, and Alexei A Efros. Context encoders: Feature learning by inpainting. In *IEEE Conf. Comput. Vis. Pattern Recog.*, pages 2536–2544, 2016. [2](#)
- [51] Pierluigi Zama Ramirez, Matteo Poggi, Fabio Tosi, Stefano Mattoccia, and Luigi Di Stefano. Geometry meets semantics for semi-supervised monocular depth estimation. In *Asian Conf. Comput. Vis.*, pages 298–313, 2018. [3](#)
- [52] Olaf Ronneberger, Philipp Fischer, and Thomas Brox. U-net: Convolutional networks for biomedical image segmentation. In *Int. Conf. Medical Image Computing and Computer-assisted Intervention*, pages 234–241, 2015. [2](#), [6](#), [12](#)
- [53] Ozan Sener and Silvio Savarese. Active learning for convolutional neural networks: A core-set approach. *arXiv preprint arXiv:1708.00489*, 2017. [2](#)

- [54] Burr Settles. Active learning literature survey. Technical report, University of Wisconsin-Madison Department of Computer Sciences, 2009. [2](#)
- [55] Burr Settles and Mark Craven. An analysis of active learning strategies for sequence labeling tasks. In *Conf. Empirical Methods Natural Language Processing*, pages 1070–1079, 2008. [2](#)
- [56] H Sebastian Seung, Manfred Opper, and Haim Sompolinsky. Query by committee. In *Annual Workshop Computational Learning Theory*, pages 287–294, 1992. [2](#)
- [57] Lei Shi and Yi-Dong Shen. Diversifying convex transductive experimental design for active learning. In *IJCAI*, pages 1997–2003, 2016. [2](#)
- [58] Yawar Siddiqui, Julien Valentin, and Matthias Nießner. Viewal: Active learning with viewpoint entropy for semantic segmentation. In *IEEE Conf. Comput. Vis. Pattern Recog.*, pages 9433–9443, 2020. [2](#)
- [59] Samarth Sinha, Sayna Ebrahimi, and Trevor Darrell. Variational adversarial active learning. In *Int. Conf. Comput. Vis.*, pages 5972–5981, 2019. [2](#)
- [60] Nasim Souly, Concetto Spampinato, and Mubarak Shah. Semi supervised semantic segmentation using generative adversarial network. In *Int. Conf. Comput. Vis.*, pages 5688–5696, 2017. [2](#)
- [61] Antti Tarvainen and Harri Valpola. Mean teachers are better role models: Weight-averaged consistency targets improve semi-supervised deep learning results. In *Adv. Neural Inform. Process. Syst.*, pages 1195–1204, 2017. [2](#), [5](#)
- [62] Simon Vandenhende, Stamatios Georgoulis, Marc Proesmans, Dengxin Dai, and Luc Van Gool. Revisiting multi-task learning in the deep learning era. *arXiv preprint arXiv:2004.13379*, 2020. [1](#)
- [63] Vikas Verma, Alex Lamb, Juho Kannala, Yoshua Bengio, and David Lopez-Paz. Interpolation consistency training for semi-supervised learning. *arXiv preprint arXiv:1903.03825*, 2019. [5](#)
- [64] Xiaolong Wang and Abhinav Gupta. Unsupervised learning of visual representations using videos. In *Int. Conf. Comput. Vis.*, pages 2794–2802, 2015. [2](#)
- [65] Shuai Xie, Zunlei Feng, Ying Chen, Songtao Sun, Chao Ma, and Mingli Song. Deal: Difficulty-aware active learning for semantic segmentation. *arXiv preprint arXiv:2010.08705*, 2020. [2](#)
- [66] Dan Xu, Wanli Ouyang, Xiaogang Wang, and Nicu Sebe. Pad-net: Multi-tasks guided prediction-and-distillation network for simultaneous depth estimation and scene parsing. In *IEEE Conf. Comput. Vis. Pattern Recog.*, pages 675–684, 2018. [6](#), [12](#)
- [67] Lin Yang, Yizhe Zhang, Jianxu Chen, Siyuan Zhang, and Danny Z Chen. Suggestive annotation: A deep active learning framework for biomedical image segmentation. In *Int. Conf. Medical Image Computing and Computer-assisted Intervention*, pages 399–407, 2017. [2](#)
- [68] Fisher Yu and Vladlen Koltun. Multi-scale context aggregation by dilated convolutions. *arXiv preprint arXiv:1511.07122*, 2015. [2](#)
- [69] Kai Yu, Jinbo Bi, and Volker Tresp. Active learning via transductive experimental design. In *Int. Conf. Mach. Learning*, pages 1081–1088, 2006. [2](#)
- [70] Sangdoon Yun, Dongyoon Han, Seong Joon Oh, Sanghyuk Chun, Junsuk Choe, and Youngjoon Yoo. Cutmix: Regularization strategy to train strong classifiers with localizable features. In *Int. Conf. Comput. Vis.*, pages 6023–6032, 2019. [1](#), [4](#), [5](#)
- [71] Lijun Zhang, Chun Chen, Jiajun Bu, Deng Cai, Xiaofei He, and Thomas S Huang. Active learning based on locally linear reconstruction. *IEEE Trans. Pattern Anal. Mach. Intell.*, pages 2026–2038, 2011. [2](#)
- [72] Yu Zhang and Qiang Yang. A survey on multi-task learning. *arXiv preprint arXiv:1707.08114*, 2017. [1](#)
- [73] Hengshuang Zhao, Jianping Shi, Xiaojuan Qi, Xiaogang Wang, and Jiaya Jia. Pyramid scene parsing network. In *IEEE Conf. Comput. Vis. Pattern Recog.*, pages 2881–2890, 2017. [2](#)
- [74] Tinghui Zhou, Matthew Brown, Noah Snavely, and David G Lowe. Unsupervised learning of depth and ego-motion from video. In *IEEE Conf. Comput. Vis. Pattern Recog.*, pages 1851–1858, 2017. [1](#), [3](#)
- [75] Yuliang Zou, Zelun Luo, and Jia-Bin Huang. Df-net: Unsupervised joint learning of depth and flow using cross-task consistency. In *Eur. Conf. Comput. Vis.*, pages 36–53, 2018. [3](#)
- [76] Laurent Zwald and Sophie Lambert-Lacroix. The berhu penalty and the grouped effect. *arXiv preprint arXiv:1207.6868*, 2012. [12](#)

A. Further Implementation Details

In the following paragraphs, a more detailed description of the network architecture and the training is provided. The reference implementation is available at https://github.com/lhoyer/improving_segmentation_with_selfsupervised_depth.

Network Architecture The neural network combines a DeepLabv3 [5] with a U-Net [52] style decoder for depth and segmentation prediction each. As encoder, a ResNet101 with dilated (instead of strided) convolutions in the last block is used. Features from multiple scales are aggregated by an ASPP [5] block with dilation rates of 6, 12, and 18. For the decoder, we use a U-Net architecture [52], which has five upsampling blocks with skip connections. Each upsampling block consist of a 3x3 convolution layer (except the first block, which is the ASPP), a bilinear up-sampling operation, a concatenation with the encoder features of corresponding size (skip connection) and another 3x3 convolution layer. Both convolutional layers are followed by an ELU non-linearity. The number of output channels for the blocks are 256, 256, 128, 128, and 64. The last four blocks also have another 3x3 convolutional layer followed by a sigmoid activation attached to their output for the purpose of predicting the disparity at the respective scale. For effective multi-task learning, we additionally follow PAD-Net [66] and deploy an attention guided multi modal distillation module with additional side output for semantic segmentation after the third decoder block. In experiments without multi-task learning, only the semantic segmentation decoder is used. For pose estimation, we use a lightweight ResNet18 encoder followed by four convolutions to produce the translation and the rotation in an angle-axis representation as suggested in [17].

Runtime To give an impression of the computational complexity of our architecture, we provide the training time per iteration and the inference time per image on a Nvidia Tesla P100 in Tab. S4. The values are averaged over 100 iterations or 500 images, respectively. Please note that these timings include the computational overhead of the training framework such as logging and validation metric calculation.

Data Selection In the data selection experiment, we use a slimmed network architecture for f_{SIDE} with a ResNet50 backbone, 256, 128, 128, 64, and 64 decoder channels, and BatchNorm [25] in the decoder for efficiency and faster convergence. The depth student network is trained using a berHu loss [76, 33]. The quality of the selected subset with annotations is evaluated for semantic segmentation using our default architecture and training hyperparameters.

Table S4. Runtimes on a Nvidia Tesla P100 averaged over 100 iterations or 500 images, respectively. D-P: SDE Transfer Learning (Pretraining), D-M SDE Transfer and Multi-Task Learning, T: Mean Teacher, X-D: Mix Depth

D	T	X	Inference Time	Training Time
P			66 ms/img	188 ms/it
P	✓		67 ms/img	466 ms/it
P	✓	D	66 ms/img	476 ms/it
M	✓	D	160 ms/img	1215 ms/it

B. Cross-Dataset Transfer Learning

In this section, we show that the unlabeled image sequences and the labeled segmentations can also originate from different datasets within similar visual domains. For that purpose, we train the SDE on Cityscapes sequences and learn the semi-supervised semantic segmentation on the CamVid dataset [2], which contains 367 train, 101 validation, and 233 test images with dense semantic segmentation labels for 11 classes from street scenes in Cambridge. To ensure a similar feature resolution, we upsample the CamVid images from 480×360 to 672×512 pixels and randomly crop to a size of 512×512 .

Table S5 shows that the results on CamVid are similar to our main results on Cityscapes. For 50 labeled training samples, SDE pretraining improves the mIoU by 3.6 percent point, Mean Teacher and DepthMix by another 4.06 percent point, and data selection by another 1.08 percent point. In the end, our proposed method significantly outperforms ClassMix by 2.01 percent point for 50 labeled samples and 1.9 percent point for 100 labeled samples. Also for the fully labeled dataset, our method can improve the performance by 3.29 percent point.

C. Further Example Predictions

Further examples of the semantic segmentation as well as the SDE are shown in Fig. S5. In general, the same observations as in the main paper can be made. Our method provides clearer segmentation contours for objects that are bordered by pronounced depth discontinuities such as pole, traffic sign, or traffic light. We also show improved differentiation between similar classes such as truck, bus, and train. On the downside, SDE sometimes fails for cars driving directly in front of the camera (see 7th row in Fig. S5) and violating the reconstruction assumptions. Those cars are observed at the exact same location across the image sequence and can not be correctly reconstructed during SDE training, even with correct depth and pose estimates. However, this differentiation between moving and non-moving cars does not hinder the transfer of SDE-learned features to semantic segmentation, but can cause problems with DepthMix (see Section D).

Table S5. Performance on the CamVid test set (mIoU in %, standard deviation over 3 random seeds). The SDE is trained on Cityscapes sequences. DP: SDE Transfer Learning, XD - DepthMix, S: Data Selection.

# Labeled	50		100		367 (Full)	
Baseline	59.16 \pm 1.79	\rightarrow	63.05 \pm 0.59	\rightarrow	68.18 \pm 0.13	\rightarrow
Ours (DP)	62.75 \pm 2.32	+3.60	66.19 \pm 0.96	+3.15	70.45 \pm 0.35	+2.27
ClassMix [47]	65.89 \pm 0.33	+6.73	67.48 \pm 1.02	+4.43	-	-
Ours (DP+XD)	66.82 \pm 1.16	+7.66	68.91 \pm 0.62	+5.86	71.46 \pm 0.22	+3.29
Ours (DP+XD+S)	67.90 \pm 0.69	+8.74	69.38 \pm 0.64	+6.33	-	-

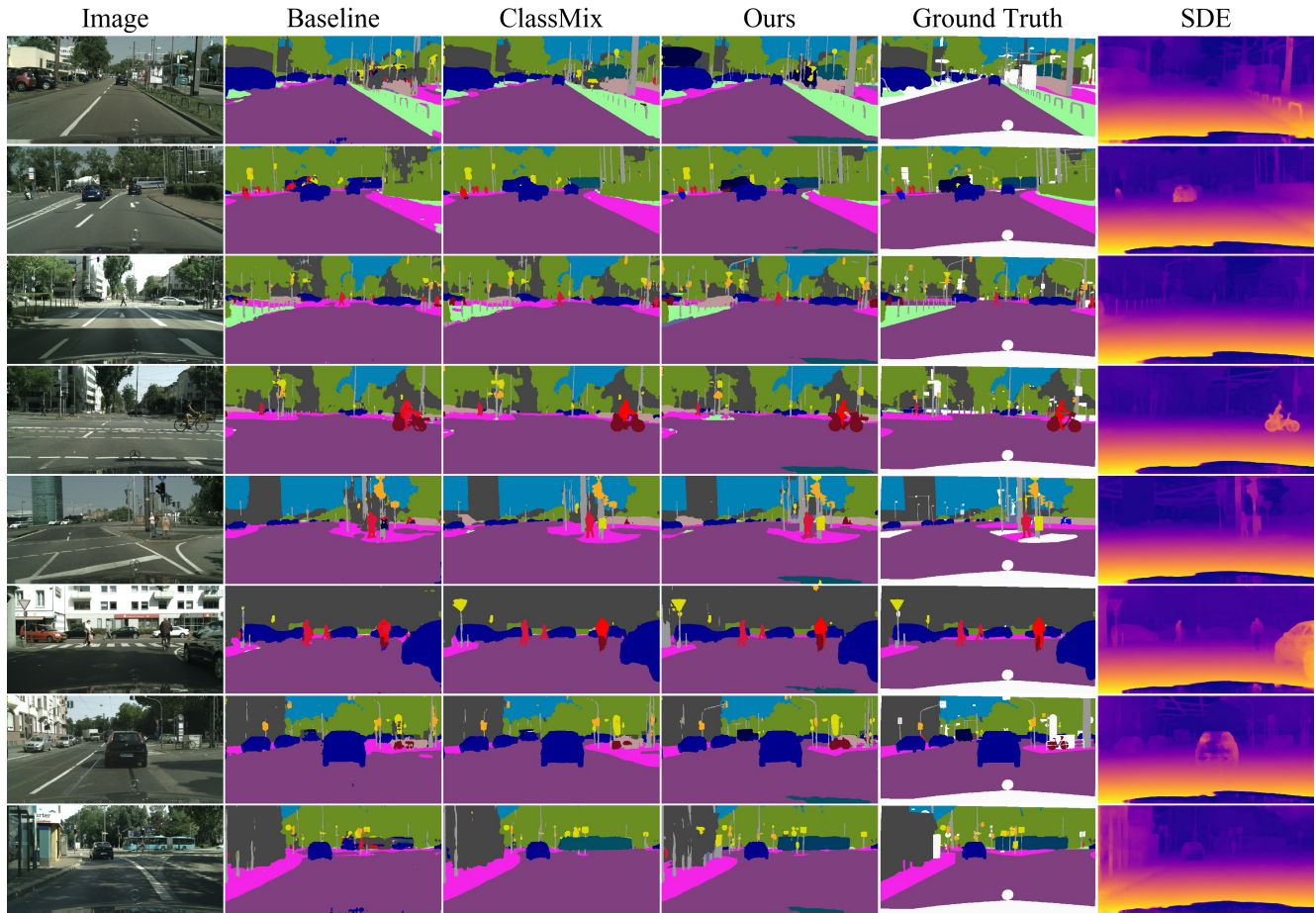


Figure S5. Further example predictions for 100 annotated training samples including the self-supervised disparity estimate of the multi-task framework.

D. DepthMix Real-World Examples

In Fig. S6 we show examples of DepthMix applied to Cityscapes crops. Generally, it can be seen that DepthMix works well in most cases. The self-supervised depth estimates allow to correctly model occlusions and the produced synthetic samples have a realistic appearance.

In Fig. S7 we show a selection of typical failure cases of DepthMix. First, the SDE can be inaccurate for dynamic objects (see Sec. C), which can cause an inaccurate structure within the mixed image (Fig. S7 a, b, and c). However, this type of failure case is common in ClassMix and its fre-

quency is greatly reduced with DepthMix. A remedy might be SDE extensions that model the motion of dynamic objects [3, 10, 32]. Second, in some cases, the SDE can be imprecise and the depth discontinuities do not appear at the same location as the class border. This can cause artifacts in the mixed image (Fig. S7 d and e) but also in the mixed segmentation (Fig. S7 e: sky within the building). Note that the same can happen for ClassMix when using pseudo labels for creating the mix mask.

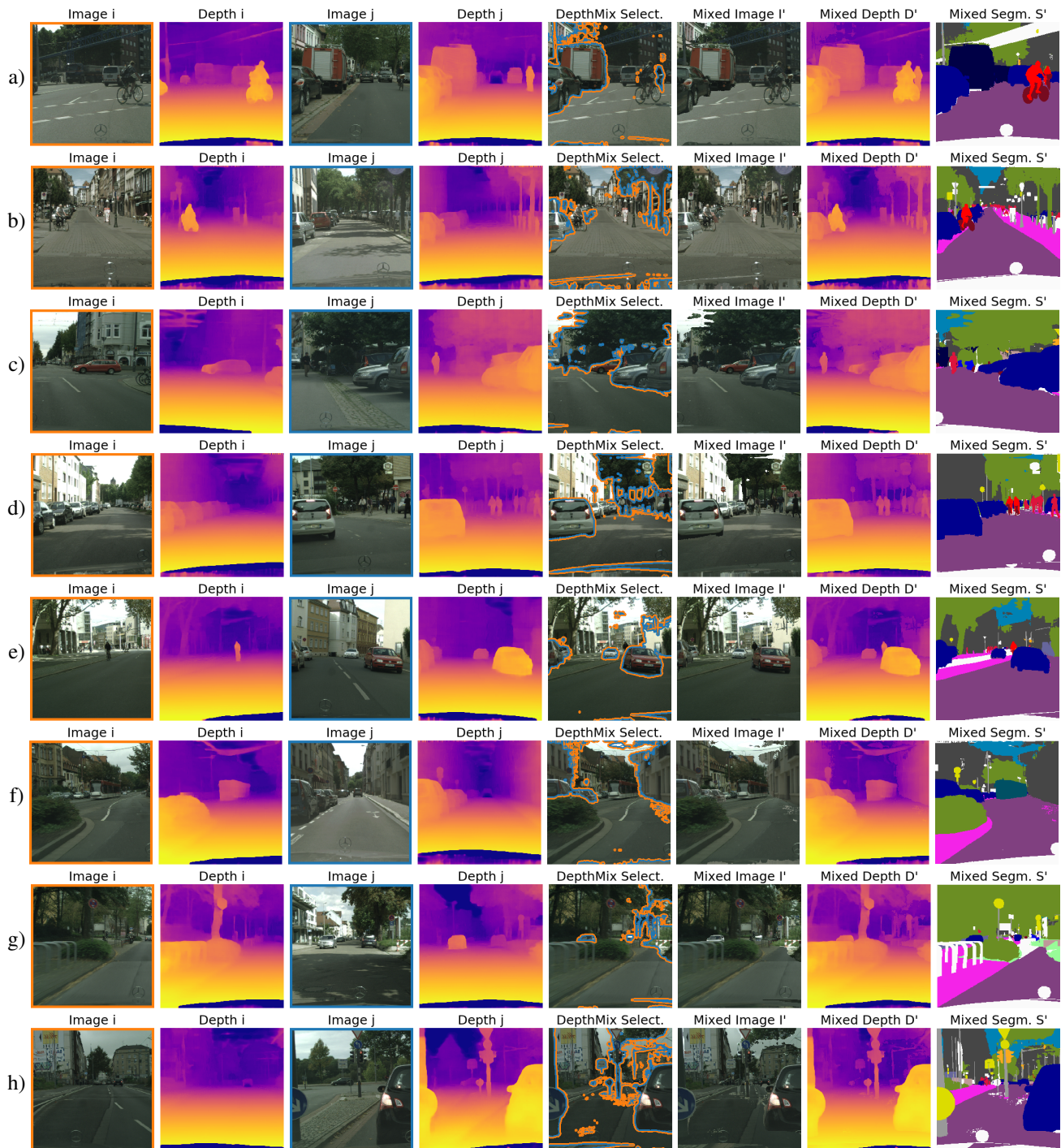


Figure S6. DepthMix applied to Cityscapes crops. From left to right, the source images with their SDE estimate, the mixed image I' overlaid with border of the mix mask M in blue/orange depending on the adjacent source image (i - orange, j - blue), the mixed image without visual guidance I' , the mixed depth D' , and the mixed segmentation S' are shown. For simplicity, the source segmentations for the mixed segmentation S' originate from the ground truth labels.

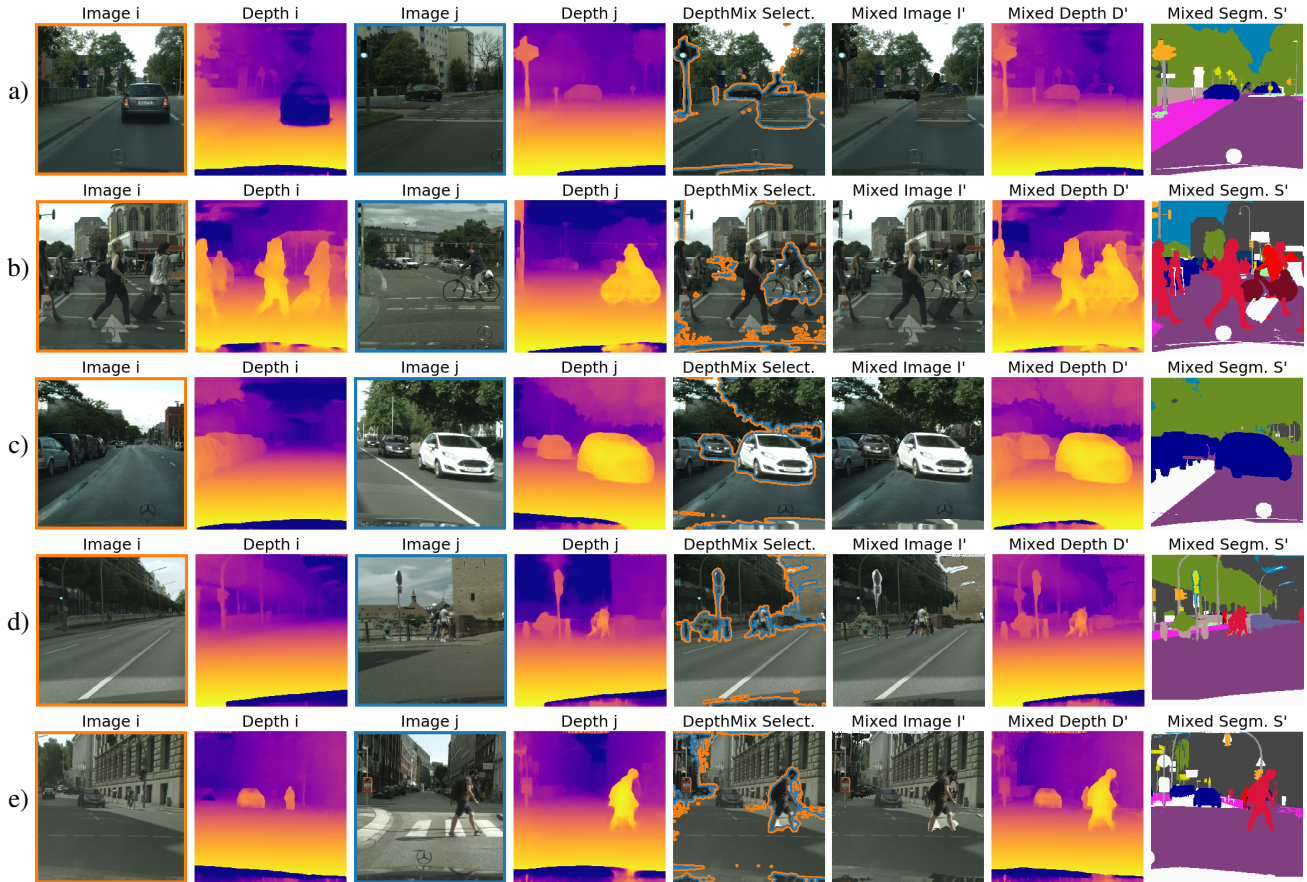


Figure S7. DepthMix failure cases. From left to right, the source images with their SDE estimate, the mixed image I' overlaid with border of the mix mask M in blue/orange depending on the adjacent source image (i - orange, j - blue), the mixed image without visual guidance I' , the mixed depth D' , and the mixed segmentation S' are shown. For simplicity, the source segmentations for the mixed segmentation S' originate from the ground truth labels.